Portable Gait Lab: Tracking Relative Distances of Feet and CoM Using Three IMUs

Mohamed Irfan Mohamed Refai, *Member, IEEE*, Bert-Jan F. van Beijnum, *Member, IEEE*, Jaap H. Buurke, and Peter H. Veltink, *Senior Member, IEEE*

***Abstract*— Ambulatory estimation of gait and balance parameters requires knowledge of relative feet and centre of mass (CoM) positions. Inertial measurement units (IMU) placed on each foot, and on the pelvis are useful in tracking these segments over time, but cannot track the relative distances between these segments. Further, drift due to strapdown inertial navigation results in erroneous relative estimates of feet and CoM positions after a few steps. In this study, we track the relative distances using the assumptions of the Centroidal Moment Pivot (CMP) theory. An Extended Kalman filter approach was used to fuse information from different sources: strapdown inertial navigation, commonly used constraints such as zero velocity updates, and relative segment distances from the CMP assumption; to eventually track relative feet and CoM positions. These estimates were expressed in a reference frame defined by the heading of each step. The validity of this approach was tested on variable gait. The step lengths and step widths were estimated with an average absolute error of 4.6±1.5 cm and 3.8±1.5 cm respectively when compared against the reference VICON©. Additionally, we validated the relative distances of the feet and the CoM, and further, show that the approach proves useful in identifying asymmetric gait patterns. We conclude that a three IMU approach is feasible as a portable gait lab for ambulatory measurement of foot and CoM positions in daily life.**

***Index Terms*— Inertial measurement unit, gait analysis, step length, relative feet distance, CoM kinematics.**

I. Introduction

GAIT kinematics and kinetics are necessary for assessing spatio-temporal as well as qualitative metrics such as Base of Support (BoS), and Margin of Stability (MoS), that are useful in assessing dynamic balance [1]. Ambulatory assessment of these parameters helps us understand gait biomechanics outside the restricted laboratory environment, providing potential applications in daily life monitoring.

Manuscript received April 8, 2020; revised July 13, 2020 and July 29, 2020; accepted August 4, 2020. Date of publication August 20, 2020; date of current version October 8, 2020. This work was supported in part by the Netherlands Organisation for Scientific Research (NWO) through the Perspectief Programme NeuroCIMT under Project 14905. *(Corresponding author: Mohamed Irfan Mohamed Refai.)*

Mohamed Irfan Mohamed Refai, Bert-Jan F. van Beijnum, and Peter H. Veltink are with the Department of Biomedical Signals and Systems, University of Twente, 7522 NB Enschede, The Netherlands (e-mail: m.i.mohamedrefai@utwente.nl).

Jaap H. Buurke is with the Roessingh Research and Development, 7522 AH Enschede, The Netherlands, and also with the Department of Biomedical Signals and Systems, University of Twente, 7522 NB Enschede, The Netherlands.

Digital Object Identifier 10.1109/TNSRE.2020.3018158

A minimal inertial measurement units (IMU) only approach has great benefits as an ambulatory sensing setup; they are highly portable and can be miniaturised. They are suitable for measuring kinematics of any rigid body segment they are attached to using strapdown inertial navigation. However, this introduces errors in the position estimates. Further, IMUs do not track relative distances from nearby body segments. This results in erroneous estimates of relative distances of segments over time. There are different solutions to solve this issue of drift between two segments. For instance, Xsens^{TM} offers a full body suit of IMUs that employ a biomechanical chain [2] to track movement of associated body segments. This requires setting up a lot of IMUs, and initializing a few biomechanical parameters. Alternatively, specially designed systems such as the ForceShoe^{TM} [3], and SWING [4] use time of flight information from ultrasound or infrared respectively, to measure the relative distance between the feet. Unfortunately, the ForceShoe^{TM} is quite thick and heavy, and not suited for daily wear [1]. Also, additional sensors require extra calibration and synchronisation steps for reliable monitoring.

A minimal three IMU setup, where one IMU is placed on each foot and one on the pelvis is an ideal setup for ambulatory monitoring. However, this may be insufficient for measuring relative foot and pelvis positions, owing to the issue of drift described earlier. Some studies solve this by using mathematical constraints that prevents drift between the feet [5], [6]. However, these may not reflect the true foot positions during continuous tracking, or in cases of an asymmetric gait. Other studies use biomechanical constraints related to the pattern of gait. Bancroft and Lachapelle [7] use information about stride length, and a difference in vector between foot positions to reduce the drift. Zhao *et al.* [8] use a derivation of step length from information about limb sway for this purpose. In both cases, approximations have been made regarding a general pattern of gait cycle. Sy *et al.* [9] show that using an extended set of biomechanical constraints can help estimate kinematics from a reduced sensor setup, but they assume a fixed pelvis, and do not comment on relative segment distances.

The theory of Centroidal Moment Pivot (CMP) could serve as a realistic biomechanical principle that relates the movement of the CoM with the stance foot. Assuming an inverted pendulum model of gait, the theory states that for normal, level-ground human walking, the moments around the CoM

is zero [10], [11]. This implies that the whole body ground reaction force (GRF) and a vector connecting the virtual CMP point and CoM are parallel [12]. This gives us a relation between the virtual CMP point and CoM, and that of the GRF [12]. For an IMU based approach, the virtual CMP point can be assumed to be the same as foot position. Additionally, estimations of the shear GRF and the height of the CoM are required [12]. Using the pelvis IMU, the 3D GRF can be estimated [13], and the height of the CoM can be tracked by adapting existing methods in literature [14], [15].

The goal of this study is to track the relative positions of the feet and CoM using only three IMUs. For this, first, the foot trajectories were estimated from the foot IMUs using strapdown integration, improved by zero velocity and zero height updates [3]. Then, the 3D instantaneous estimates of GRF [13], CoM velocity [16], and height [14] were estimated from the pelvis IMU. 3D GRF and CoM height were used to solve the CMP theory, and derive relative positions between the feet and CoM [12]. These positions were used to reduce the drift between the feet and CoM. The proposed algorithm was tested for variable gait patterns. The resulting kinematics were expressed in a body-centric frame of reference or current step frame [13], and compared with reference systems.

II. Methods

Here, the methods used to track the kinematics of feet and CoM are further explained. First, in Section II-A, we briefly explain the reference frames [13] used in this study. Next, Section II-B describes the IMU models used. In Section II-C, the design of the EKF for the tracking is described. Section II-D describes the measurement systems used, and Sections II-E and II-F describe the participant group, and the experimental protocol used to obtain measurements and validate this study respectively. Finally, Section II-G explains how the results were analysed.

A. Reference Frames Used

A changing reference frame [13] was used to express the kinematics in this study. This allows us to provide a body centric frame of expression, as opposed to an arbitrary global frame used commonly. A detailed description of the different frames used and the transformations between them are given in Mohamed Refai *et al.* [13]. Here, we summarize them briefly.

The changing reference frame was based on the direction of steps being made and will be referred to as the current step frame, denoted as ψ_{cs}. In Fig. 1, an example of ψ_{cs} for the step k made by the right leg is shown as the light green shaded triangle. The frame was defined with the X axis along the heading of the step (bold dotted line in Fig. 1) and Z along the vertical. As the IMU measures in its sensor frames, ψ_s, it has to be transfomed to the ψ_{cs} per step.

First, a sensor to segment calibration was performed to the respective segment (*seg*) frames ψ_{seg} [13]. The segments included the pelvis (*p*), left foot (*fl*), and the right foot (*fr*). Then, the change in orientation of the segments during a step k was first expressed in the current step frame $\psi_{cs(k-1)}$ of the previous step $k-1$. The change in orientation was estimated

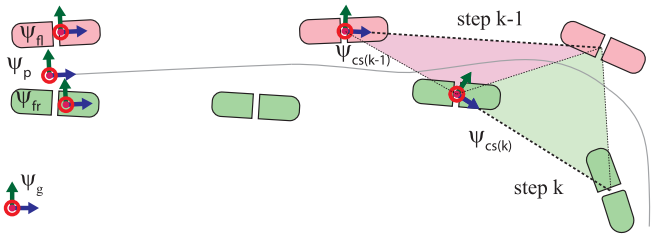

Fig. 1. Graphical interpretation of the reference frames used [13]. The pink foot is the left foot, and the thin line is the CoM trajectory during walking. The changing current step frame $\psi_{cs(k)}$ is defined for each step *k*. Segments of interest were the feet (*fl*) and (*fr*), and pelvis (*p*).

using an error extended Kalman filter [13]. At the end of the step k, using the change in position of the swing foot the $\psi_{cs(k)}$ was estimated. This procedure was iterated for each step.

In short, four frames of reference were used in this study: sensor frame (ψ_s), segment frames (pelvis ψ_p, right foot ψ_{fl} and left foot ψ_{fl}), a current step frame defined by the previous step ($\psi_{cs(k-1)}$), and the current step k ($\psi_{cs(k)}$).

B. Inertial Measurement Unit Model

The 3D accelerometer and 3D rate gyroscope present in the IMU provides the acceleration and angular velocities in the sensor frame ψ_s respectively, and can be modelled as:

$$\mathbf{y}_A^s = \mathbf{a}^s - \mathbf{g}^s + \mathbf{e}_A \tag{1}$$

$$\mathbf{y}_G^s = \boldsymbol{\omega}^s + \mathbf{b}^s + \mathbf{e}_G \tag{2}$$

Here, $\mathbf{a}$ is the linear acceleration of the sensor, $\mathbf{g}$ is gravity, and $\mathbf{e}_A$ is Gaussian white noise. Also, $\boldsymbol{\omega}$ is the angular velocity, $\mathbf{b}$ is a slowly varying offset, and $\mathbf{e}_G$ is Gaussian noise. Both (1) and (2) are discrete time equations and are expressed for a given time instance i.

C. Fusion Filter to Track Relative Feet and CoM Positions

Fig. 2 shows a brief overview of the steps involved. There are a few working assumptions we need to consider. We assumed an inverted pendulum model of gait where all mass is concentrated at the CoM that is located within the pelvis [11], [15]. Thus, the GRF accelerates the CoM and opposes gravity. These assumptions should hold as long as the subject walks normally, and doesn't fall or negotiate large obstacles. Additionally, the feet are the only contact with the external world, and no additional load is carried by the body. Given these assumptions, the accelerations measured by the IMU at the pelvis is similar to the accelerations at the CoM. Thereby, the pelvis segment (p) will be hereto referred as the CoM (C).

The method of Skog *et al.* [17] was used to estimate the foot contact instances for each foot. As the IMUs were synchronized in time, double stance instances can be estimated. Though, distinct gait events can be estimated from foot IMUs [18], for sake of simplicity, a step was defined to take place between halfway of a double stance until halfway of the subsequent double stance.

TABLE I
NOTATIONS USED, FOR AN ARBITRARY VECTOR **a**

Notation	Definition
$\mathbf{a}_k$	k-th instant
$\mathbf{a}^s$	vector **a** expressed in frame ψ_s
$\dot{\mathbf{a}}$	derivative of **a**
$\hat{\mathbf{a}}$	a posteriori estimate of **a**
$\mathbf{a}^-$	a priori of **a**
$\mathbf{e_a}$	Gaussian white noise associated with **a**

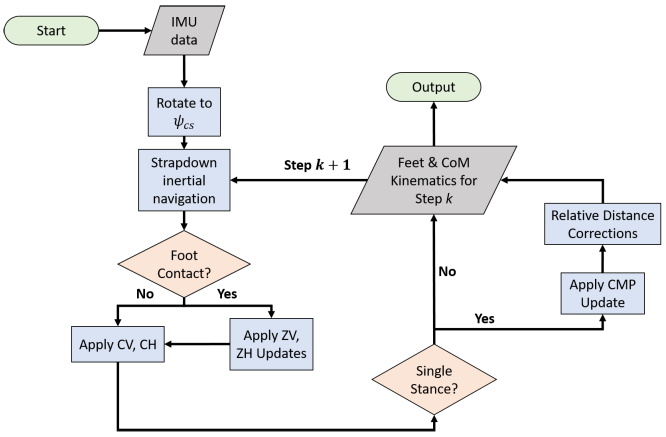

Fig. 2. Overview of Sensor fusion filter design. Measurement updates used are zero velocity (ZV), zero height (ZH), CoM velocity (CV), CoM height (CH), and Centroidal Moment Pivot (CMP).

An extended Kalman filter (EKF) was used to track the velocity and position of the three segments; both feet and CoM, in the current step frame ψ_{cs}. The filter notations used are tabulated in Table I. The state vector of the EKF was denoted as $\mathbf{x}$ and its covariance matrix as $\mathbf{P}$. The states as shown in (3) included the 3D position $\mathbf{p}$, and 3D velocity $\mathbf{v}$ of each segment, with the superscript denoting the corresponding segment.

$$\mathbf{x} = (\mathbf{p}^{fr} \quad \mathbf{p}^{fl} \quad \mathbf{p}^{C} \quad \mathbf{v}^{fr} \quad \mathbf{v}^{fl} \quad \mathbf{v}^{C})^T \tag{3}$$

The following text expands on the overview shown in Fig. 2. It describes the a-priori estimate determined using strapdown integration of the accelerations measured at each segment. Then, the special biomechanical constraints applied to each segment are shown. The implementation of the CMP assumptions to reduce the drift between the three segments is also described.

1) Strapdown Inertial Navigation: This is the prediction step of the EKF. The accelerations at each segment was expressed in the $\psi_{cs(k)}$ as [13]:

$$\begin{aligned}\hat{\mathbf{a}}_i^{cs(k)} &= \mathbf{R}_k^{cs(k),cs(k-1)}(\mathbf{R}_i^{cs(k-1),seg}\hat{\mathbf{a}}_i^{seg}) \\ &= \mathbf{R}_k^{cs(k),cs(k-1)}(\mathbf{R}_i^{cs(k-1),seg}(\mathbf{y}_{A,i}^{seg} + \mathbf{g}^{seg})) \\ &= \mathbf{R}_k^{cs(k),cs(k-1)}(\mathbf{R}_i^{cs(k-1),seg} \cdot \mathbf{y}_{A,i}^{seg} + \mathbf{g}^{cs(k-1)})\end{aligned} \tag{4}$$

The $\mathbf{R}_k^{cs(k),cs(k-1)}$, and $\mathbf{R}_i^{cs(k-1),seg}$ were estimated using the methods described in Section II-A [13]. Here, i denotes the samples during the current step k. The position and velocity can be estimated as [3]:

$$\hat{\mathbf{v}}_i^{cs} = \hat{\mathbf{v}}_{i-1}^{cs} + T\hat{\mathbf{a}}_i^{cs} \tag{5}$$

$$\hat{\mathbf{p}}_i^{cs} = \hat{\mathbf{p}}_{i-1}^{cs} + T\hat{\mathbf{v}}_i^{cs} + \frac{T^2}{2}\hat{\mathbf{a}}_i^{cs} \tag{6}$$

Here, T is the time step. The Kalman filter prediction equation was given as [19]:

$$\hat{\mathbf{x}}_i^- = \mathbf{F}\hat{\mathbf{x}}_{i-1} + \mathbf{u}_{i-1} \tag{7}$$

$$\text{where } \mathbf{F} = \begin{pmatrix}\mathbf{I}_3 & T \\ \mathbf{0}_3 & \mathbf{I}_3\end{pmatrix}, \text{ and } \mathbf{u} = \begin{pmatrix}\frac{T^2}{2} \cdot \hat{\mathbf{a}}_i^{cs} \\ T \cdot \hat{\mathbf{a}}_i^{cs}\end{pmatrix} \tag{8}$$

and the covariance matrix was predicted using

$$\hat{\mathbf{P}}_i^- = \mathbf{F}\hat{\mathbf{P}}_{i-1}\mathbf{F}^T + \mathbf{Q} \tag{9}$$

where, $\mathbf{Q}$ is the process noise covariance matrix.

2) Measurement Update: The measurement updates used to reduced drift in the estimation of position and velocity of the feet and CoM are as follows. A summary of when these updates are applied is shown in Fig. 2.

- *Zero Velocity Update (ZV)*: As shown in Fig. 2, this is applied when the foot is in contact with the ground [17], as the velocity of the feet are assumed to be zero. The measurement $\mathbf{z}_{zv}$ is provided as follows, and applied only to the feet.

$$\mathbf{z}_{zv} = \mathbf{0}_{3\text{x}1} \tag{10a}$$
$$\hat{\mathbf{z}}_{zv} = \mathbf{H}_{zv} \cdot \hat{\mathbf{x}}^- + \mathbf{e}_{zv} \tag{10b}$$
$$\text{with, } \mathbf{H}_{zv}^{fr} = (\mathbf{0}_{3\text{x}9} \ \mathbf{I}_{3\text{x}3} \ \mathbf{0}_{3\text{x}6}) \tag{10c}$$
$$\text{and, } \mathbf{H}_{zv}^{fl} = (\mathbf{0}_{3\text{x}12} \ \mathbf{I}_{3\text{x}3} \ \mathbf{0}_{3\text{x}3}) \tag{10d}$$

  In the above equations, $\mathbf{H}$ transforms the state vector to a measurement prediction $\hat{\mathbf{z}}$, and $\mathbf{z}$ denotes the actual measurement [19]. $\mathbf{e}_{zv}$ denotes the error associated with this measurement. The same notations are used in the following equations.
- *Zero Height Update (ZH)*: During the same foot contact instances as above, if we assume walking over a flat surface, we have information regarding the height of the foot from the floor.

$$\mathbf{z}_{zh} = p_{Z,init}^f \tag{11a}$$
$$\hat{\mathbf{z}}_{zh} = \mathbf{H}_{zh} \cdot \hat{\mathbf{x}}^- + \mathbf{e}_{zh} \tag{11b}$$
$$\text{with, } \mathbf{H}_{zh}^{fr} = (0\ 0\ 1\ 0\ 0\ 0\ \mathbf{0}_{1\text{x}15}) \tag{11c}$$
$$\text{and, } \mathbf{H}_{zh}^{fl} = (0\ 0\ 0\ 0\ 0\ 1\ \ \mathbf{0}_{1\text{x}12}) \tag{11d}$$

  The measurement matrix $\mathbf{H}_{zh}$ has only one row as it transforms only the Z axis of each foot. Here, $\mathbf{p}_{Z,init}^f$ is the initial height and the superscript f denotes either the left (fl) or right foot (fr). This update was only applied to the feet.
- *CoM Velocity (CV)*: The ZV update ensures that the velocity of the feet do not drift due to integration errors. However, the CoM is constantly moving. Therefore, an estimate of the CoM velocity was derived by fusing two complementary sources of information [11], [16]. A high frequency information ($\mathbf{v}_{hf}^C$) was derived from

an optimally filtered direct and reverse strapdown integration [14] of the CoM accelerations using a cut off of 0.6 Hz. Then, low frequency information ($\mathbf{v}^C_{lf}$) of the CoM velocity was derived from low pass filtering the average of the foot velocities using the same cut off used for $\mathbf{v}^C_{hf}$. The two sources were fused to get estimates of the instantaneous 3D CoM velocity [16]:

$$\mathbf{v}^C = \mathbf{v}^C_{lf} + \mathbf{v}^C_{hf} \tag{12}$$

- *CoM Height (CH)*: The height of the CoM ($\mathbf{p}^C_Z$) was also estimated using a complementary filter method [11]. An optimally filtered direct and reverse strapdown integration [14] of vertical CoM velocity was used to obtain the changes in CoM height during gait using a cut off of 0.3 Hz to obtain the $\mathbf{p}^C_{Z,hf}$. Then, as the subject does not crouch or jump while walking, the height of the CoM should oscillate around an offset. Assuming an average walking CoM height as 98% of the height during quiet standing ($\mathbf{p}^C_{Z,init}$) showed least errors when validating this method. The average height and the $\mathbf{p}^C_{Z,hf}$ were fused to get an estimate of CoM height $\mathbf{p}^C_Z$ during walking.

$$\mathbf{p}^C_Z = 0.98 * \mathbf{p}^C_{Z,init} + \mathbf{p}^C_{Z,hf} \tag{13}$$

- *Centroidal Moment Pivot Update (CMP)*: The CMP update was used to restrict the feet and CoM from drifting apart or towards each other. Fig. 2 summarizes the steps involved; the CMP update was used to first estimate the horizontal position of stance foot with respect to the movement of the CoM. After correcting discrete changes at the start of each swing phase, the CoM trajectory was updated for the corrected foot positions. These steps are explained further below.

$$\mathbf{cmp}^f_{ax} = \mathbf{p}^C_{ax} - (\mathbf{p}^C_Z \cdot \frac{F_{ax}}{F_Z}) \tag{14}$$

(14) is a mathematical expression of the CMP theory [10]. When the 3D components of GRF are known, the distance between the CoM ($\mathbf{p}^C_{ax}$) and a virtual CMP point ($\mathbf{cmp}^f_{ax}$) under the stance foot can be estimated [13]. Here, ax denotes either X or Y axes, and F is the 3D GRF in a specific axis. The 3D components of GRF estimated from the CoM accelerations [13] were used to estimate the ratio F_{ax}/F_Z. The $\mathbf{p}^C_Z$ or height of the CoM was already estimated using the update *CH* in (13). Note that there are a few assumptions regarding (14). First, we assumed that the virtual CMP position ($\mathbf{cmp}^f_{ax}$) coincides with the stance foot positions ($\mathbf{p}^f_{ax}$) tracked by the IMU. Secondly, we assumed that the moment of inertia around the trunk is negligible while walking. Thus, during single stance phase, (14) provides the relation between CoM and $\mathbf{p}^f_{ax}$, the stance foot. This can be used as measurement updates $\mathbf{z}^{fr}_{cmr}$ and $\mathbf{z}^{fl}_{cml}$ for either foot as follows:

During left swing:

$$\mathbf{z}^{fr}_{cmr} = \mathbf{cmp}^{fr}_{ax} \tag{15a}$$
$$\hat{\mathbf{z}}^{fr}_{cmr} = \mathbf{H}^{fr}_{cmr} \cdot \hat{\mathbf{x}}^- + \mathbf{e}^{fr}_{cmr} \tag{15b}$$
$$\text{with, } \mathbf{H}^{fr}_{cmr} = (\mathbf{I}_{2\text{x}2} \;\; \mathbf{0}_{2\text{x}16}) \tag{15c}$$

During right swing:

$$\mathbf{z}^{fl}_{cml} = \mathbf{cmp}^{fl}_{ax} \tag{15d}$$
$$\hat{\mathbf{z}}^{fl}_{cml} = \mathbf{H}^{fl}_{cml} \cdot \hat{\mathbf{x}}^- + \mathbf{e}^{fl}_{cml} \tag{15e}$$
$$\text{with, } \mathbf{H}^{fl}_{cml} = (\mathbf{0}_{2\text{x}3} \;\; \mathbf{I}_{2\text{x}2} \;\; \mathbf{0}_{2\text{x}13}) \tag{15f}$$

The measurement matrices $\mathbf{H}^{fr}_{cmr}$ and $\mathbf{H}^{fl}_{cml}$ transform only the X and Y axes of the foot positions in the state vector. This update corrects the drift in relative positions between the CoM and stance foot during swing phase. However, this may cause a discrete jump in relative foot distances at the start of the swing phase. To have a smooth change in relative foot distances between subsequent steps, knowledge of the relative foot distances at the end of the preceeding step was used to update the relative foot distances at the beginning of the subsequent swing phase.

Start of left swing:

$$\mathbf{z}^{fr}_{rdr} = \mathbf{p}^{fr}_{ax,ed} \tag{16a}$$
$$\hat{\mathbf{z}}^{fr}_{rdr} = \mathbf{H}^{fr}_{rdr} \cdot \hat{\mathbf{x}}^- + \mathbf{e}^{fr}_{rdr} \tag{16b}$$
$$\text{with, } \mathbf{H}^{fr}_{rdr} = (\mathbf{I}_{2\text{x}2} \;\; \mathbf{0}_{2\text{x}16}) \tag{16c}$$

Start of right swing:

$$\mathbf{z}^{fl}_{rdl} = \mathbf{p}^{fl}_{ax,ed} \tag{16d}$$
$$\hat{\mathbf{z}}^{fl}_{rdl} = \mathbf{H}^{fl}_{rdl} \cdot \hat{\mathbf{x}}^- + \mathbf{e}^{fl}_{rdl} \tag{16e}$$
$$\text{with, } \mathbf{H}^{fl}_{rdl} = (\mathbf{0}_{2\text{x}3} \;\; \mathbf{I}_{2\text{x}2} \;\; \mathbf{0}_{2\text{x}13}) \tag{16f}$$

In (16a) and (16d), $\mathbf{p}^{fr}_{ax,ed}$ and $\mathbf{p}^{fl}_{ax,ed}$ are the respective foot positions at the end of the preceding step in the axis ax. As in (15), the measurement matrices $\mathbf{H}^{fr}_{rdr}$ and $\mathbf{H}^{fl}_{rdl}$ transform only the X and Y axes of the foot positions. This correction of relative foot distances requires a final update of the CoM position following the CMP theory. (14) was adapted to obtain the CoM from foot estimates as follows.

$$\mathbf{p}^C_{ax} = \mathbf{cmp}^f_{ax} + (\mathbf{p}^C_Z \cdot \frac{F_{ax}}{F_Z}) \tag{17}$$

During left swing, $\mathbf{cmp}^f_{ax}$ represents the right foot, and vice-versa for the right swing. During these instances, the CoM position was improved using the following measurement update:

$$\mathbf{z}^C_{cmc} = \mathbf{p}^C_{ax} \tag{18a}$$
$$\hat{\mathbf{z}}^C_{cmc} = \mathbf{H}^C_{cm} \cdot \hat{\mathbf{x}}^- + \mathbf{e}^C_{cm} \tag{18b}$$
$$\text{with, } \mathbf{H}^C_{cmc} = (\mathbf{0}_{2\text{x}6} \;\; \mathbf{I}_{2\text{x}2} \;\; \mathbf{0}_{2\text{x}10}) \tag{18c}$$

$\mathbf{p}^C_{ax}$ was derived from 17. The measurement matrix $\mathbf{H}^C_{cm}$ transforms the X and Y axes of the CoM positions to the measurement.

The measurement updates were applied to the EKF using the standard equations. The Kalman gain was estimated using (19), the state matrix was updated with (20), and the error covariance matrix was updated using (21).

$$\mathbf{K}_i = \mathbf{P}^-_i \mathbf{H}^T (\mathbf{H}\mathbf{P}^-_i \mathbf{H}^T + \mathbf{R})^{-1} \tag{19}$$
$$\hat{\mathbf{x}}_i = \hat{\mathbf{x}}^-_i + \mathbf{K}_i(\mathbf{z}_i - \mathbf{H}\hat{\mathbf{x}}^-_i) \tag{20}$$
$$\mathbf{P}_i = (\mathbf{I} - \mathbf{K}_i\mathbf{H})\mathbf{P}^-_i \tag{21}$$

TABLE II
STANDARD DEVIATIONS OF THE GAUSSIAN NOISES USED

$\mathbf{e}_G$	$\mathbf{e}_A$	$\mathbf{e}_{zv}$	$\mathbf{e}_{zh}$	$\mathbf{e}_{cml}^{fl}$ and $\mathbf{e}_{cmr}^{fr}$	$\mathbf{e}_{rdl}^{fl}$ and $\mathbf{e}_{rdr}^{fr}$	$\mathbf{e}_{cm}^{C}$
rad/s	m/s^2	*m/s*	*m*	*m*	*m*	*m*
$1 \cdot 10^{-2}$	$1 \cdot 10^{3}$	$7 \cdot 10^{-2}$	$5 \cdot 10^{-2}$	$1 \cdot 10^{1}$	$[5 \cdot 10^{-2} \quad 9 \cdot 10^{-3}]\mathbf{I}_{2x2}$	$1 \cdot 10^{-1}$

3) Reinitialising for Step k+1: After the state vector has been updated using the prediction and measurement updates, the trajectory of the segments are known for the current step k. The $\psi_{cs(k)}$ was adjusted using methods described in Section II-A using the improved estimates of the foot positions. For the next step $k+1$, accelerations are transformed to the current step frame $\psi_{cs(k+1)}$ using (4), and the steps described in Sections II-C were reiterated.

4) Initialisation and Noise: Before applying the EKF, the states for each segment and their covariance noises have to be initialised. The right foot was assumed to be the origin. The initial locations of the CoM, and the left foot were measured from VICON©. All initial velocities $\mathbf{v}_{seg}$ were set to zero, and the initial noise was set to arbitrary values. The process and measurement noises shown in Table II were estimated from sensor specifications, and then fine tuned by optimizing the error between estimated and reference values.

D. Measurement System

Three Xsens™ MTw IMUs formed the minimal setup and can be visualized in Mohamed Refai *et al.* [13]; one IMU was mounted on the pelvis, and one on each foot. The pelvis IMU was placed below the midway point between the line connecting the left and right posterior superior iliac spine. The foot IMUs were placed on the midfoot region. The MT Manager (version 4.8) software was used to read the data from the IMU wirelessly, which was sampled at 100 Hz.

Two reference systems were used. The ForceShoe™ was used as wearable reference for the estimation of forces required in (14). The ForceShoe™ consists of a 6-DoF Force and Torque sensor, and an IMU under each toe and heel of both feet [20]. It has been validated against force plates (AMTI®) for measurement of contact forces [11]. A VICON© motion capture system (Oxford Metrics PLC.) was used as the reference system for validating the velocities and positions estimated using the state vector. Markers were placed on the following locations on both the left and right limbs: anterior superior iliac spine, posterior iliac spine, the second and fifth metatarsal, and heel. One marker was also placed on each IMU. The data from VICON© and ForceShoe™ were sampled at 100 Hz. The data was then low pass filtered at 10Hz with a zero-phase second order butterworth filter.

Foot contact was estimated when the magnitude of forces measured by the ForceShoe™ was below a set threshold of 30 N on each foot. Foot positions were derived from the marker on the IMU. The CoM position obtained from VICON© was assumed to lie at the centroid of the four pelvis markers. The feet and CoM positions were differentiated and low pass filtered with a second order zero phase Butterworth filter of cut off 10 Hz to obtain the respective velocities. The measurements by both reference systems were transformed to the ψ_{cs} frame that was determined using the VICON©foot positions.

To synchronize the two reference systems with that of the Xsens™ MTw IMUs, the subjects were asked to raise their right leg before starting the experimental protocol. The magnitude of angular velocities measured with the Xsens™, as well as the IMUs in the ForceShoe™ were used to synchronize these systems. The change in right foot position was used to synchronize the VICON©with the other two systems. A manual check was performed in order to verify if all the signals were properly synchronized.

E. Participants

Six healthy subjects were recruited for the study. The average and standard deviation of the height, weight, and age was 1.7±0.1 m, 74.1±10 kg, and 25.6±2.8 years respectively. Leg length was measured from the greater trochanter to the ground [21] and was 0.9 ± 0.04 m. All participants signed an informed consent before the experiment. The study was conducted in accordance with the Declaration of Helsinki, and the protocol was approved by the Ethical Committee of the faculty. The inclusion criteria included subjects with no history of impaired gait or leg injury. One subject was female and all of their shoe sizes were 40 (European Size Chart).

F. Experimental Protocol

The ForceShoe™ was calibrated using the MT Manager software, and the VICON© was calibrated using standard procedures. Fig. 3 summarizes the experimental protocol. The subjects began by standing still for a few seconds with their feet placed parallel, and were asked to bend the trunk forward. This was used to calibrate the pelvis segment frame in Section II-A [13]. The subjects were then asked to perform a set of walking tasks, each repeated four times:

1) *Normal Walk (NW)*: The subject was asked to walk at their *preferred* walking speed for 5 m.
2) *L Walk (LW)*: The subject was asked to walk for 3 m and then turn right at 90° and walk for another 2 m.
3) *Walk and Turn (WT)*: The subject was asked to walk for 5 m and then turn and walk back to start position.
4) *Walk and Turn Twice (WT2)*: The subject performed WT and then asked to turn and walk for 5 m.
5) *Slalom Walk (SW)*: The subject was asked to walk in a slalom pattern. Two pylons, at 2 m and 4 m from start respectively, were placed on the floor to guide them.
6) *Asymmetric Walk (AW)*: The subject was asked to walk in an asymmetric manner. The instruction given was to induce a stiff left knee and abduct the hip as much as possible, and also have a shorter step on the right side.

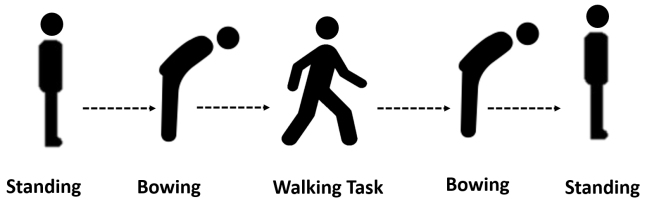

Fig. 3. Simplified overview of experimental protocol.

G. Analysis of Results

In the following text, the minimal IMU sensing setup, along with the algorithms explained in Section II-C will be referred to as Portable Gait Lab (PGL). A zero-phase Butterworth low pass filter of order 4 and cut off 3 Hz was used to filter noise from the estimated kinematics.

The estimated forces and kinematics were compared against the reference systems, ForceShoe™ and VICON© respectively. First, the errors in estimating the ratio of forces ($\frac{F_{ax}}{F_Z}$) in (14) from the pelvis IMU [13] was studied. The errors were expressed as the root mean square of the differences normalised by the range of the reference values in both X ($rRat_X$) and Y ($rRat_Y$) axis. Then, the root mean square of the differences in estimating CoM height ($RCoM_Z$) was studied. The error margins $rRat_{XZ}$, $rRat_{YZ}$, and $RCoM_Z$ are required to understand the errors associated with (14), and eventually, the relative distance estimates.

The root mean square of the errors ($Right_X$, $Right_Y$, $Left_X$, $Left_Y$, CoM_X, and CoM_Y) in estimating the horizontal positions of feet and CoM were then analysed for each step. The vertical foot clearance comparison has been neglected in this study, as it is not novel [22]. Then, the average 2D horizontal Euclidean distance (ED) between the feet at the end of each step for all walking tasks was measured and compared against the VICON© reference. Following this, spatial gait parameters, such as the Step Lengths (SL), and Step Widths (SW) were estimated [23]. A metric *CoM width* (CW) was derived by estimating the average 2D Euclidean distance between the stance foot and CoM trajectory for each step. This provided an average relative distance between either foot and CoM. Correlation and Bland-Altman plots were used to compare the SL, SW, and CW derived from the PGL with the reference VICON©. Finally, the feasibility of the PGL in differentiating between symmetrical and asymmetrical walking was studied by comparing the differences between left and right steps in two walking tasks, the NW and AW.

III. Results

A few trials were removed from analysis due to issues with the reference setups. Further, it was made sure that each subject had at least three walking trials per walking task. First, an example of the CoM height estimated using the complementary filter approach in (13) is shown in Fig. 4 as the solid blue line. The dotted red line shows the measurement by the VICON©. Here, the subject is performing a WT task and makes the 180° turn around 25 seconds. Table III shows the errors ($rRat_{XZ}$, and $rRat_{YZ}$) in estimating the ratio of forces and that of CoM height ($RCoM_Z$) in (14) for the different

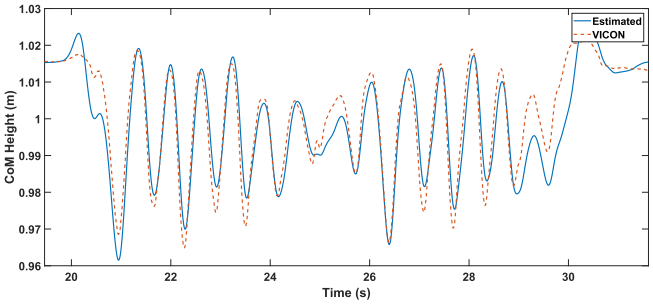

Fig. 4. Trajectory of CoM Height for a subject performing a WT task estimated from the pelvis IMU seen as solid blue line. The dotted red line is the VICON© reference.

TABLE III
Root Mean Square of the Differences in Estimating Ratio of Forces $rRat_X$, and $rRat_Y$ and CoM Height $RCoM_Z$

——	$rRat_X(\%)$	$rRat_Y(\%)$	$RCoM_Z(mm)$
NW	15 ± 3.74	16.1 ± 3.15	$6.1 \pm 0.9^*$
LW	15.2 ± 2.53	13.5 ± 3.55	$5.6 \pm 1^*$
WT	17.8 ± 2.65	15.1 ± 4.69	$5.3 \pm 1^*$
WT2	19.1 ± 2.7	15.5 ± 3.46	$7 \pm 3.1^*$
SW	17.7 ± 3.6	17.4 ± 6.84	$6.3 \pm 1^*$
AW	13 ± 2.6	19.3 ± 3.13	$11.7 \pm 4.5^*$

NW: Normal Walk, LW: L Walk, WT: Walk and Turn, WT2: Walk and Turn Twice, SW: Slalom Walk, AW: Asymmetrical Walk. *Significant ($p < 0.05$) correlations in estimated CoM height and VICON© measurement.

walking tasks. The CoM height estimations were significantly ($p < 0.05$) correlated with an average of 83 ± 8.2 % across all tasks, suggesting good agreement with the reference values.

Fig. 5 shows a graphical step-wise comparison of the feet and CoM positions estimated by the PGL with the reference VICON© for the same trial as shown in Fig. 4. In Fig. 5, circles denote estimations by the PGL, and the lines denote the measurements by VICON©. For both systems, the trajectory of the right foot is shown in red, the CoM in green, and the left foot in blue. Each subplot is a top-down view of a step expressed in the current step frame ψ_{cs}. The X axis of each plot corresponds to the X axis of the ψ_{cs}, and similarly for the Y axis. As each step is represented in its own ψ_{cs} frame, they all progress to the right, even during turns. In the first subplot, the left foot moves first. Then, the subject can be seen to make consecutive steps, until step 6, where they prepare for the 180° turn. The turning step is highlighted with a shaded light red background. Although the PGL shows deviations during the turn when compared to the reference, it converges to the reference values two steps after.

Table IV displays the errors ($Right_X$, $Right_Y$, $Left_X$, $Left_Y$, CoM_X, and CoM_Y) in estimating the horizontal feet and CoM positions for each step. These are an average across all steps in a walking task excluding the turning steps. Turning steps were those that made a 60° or larger change in direction when compared to the preceding step. Table IV also summarizes the difference in relative distance between the

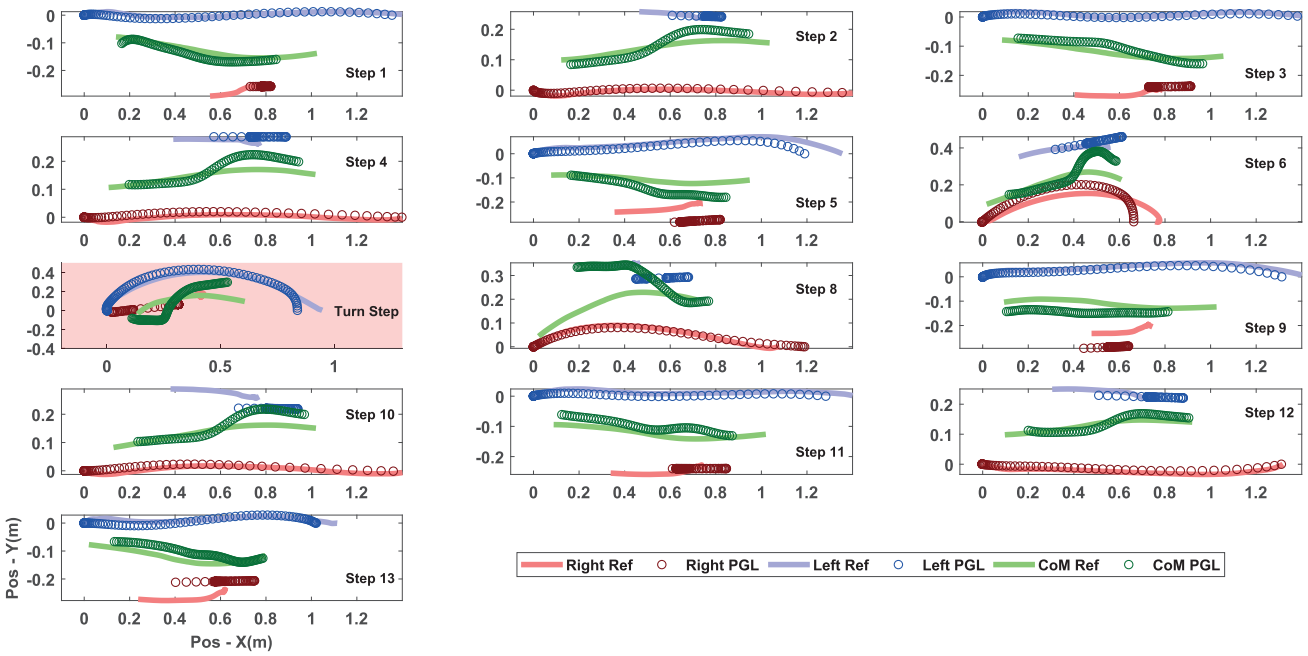

Fig. 5. Step-wise comparison of foot and CoM positions by the Portable Gait Lab (PGL) system and VICON© reference in the ψ_{cs} frame. The subject performs a WT task, with the turning step highlighted with a light red shaded background. The circles denote the PGL values, and the lines denote the reference values. In either case, positions of the right foot, left foot, and CoM are shown using red, blue, and green. The step numbers are mentioned within each plot.

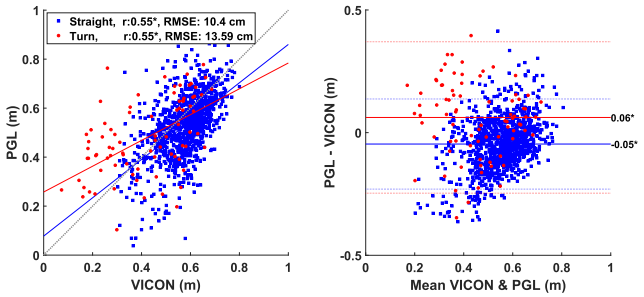

Fig. 6. Comparing step lengths using correlation and Bland-Altman plots. Red circles are turning steps. *$p < 0.05$.

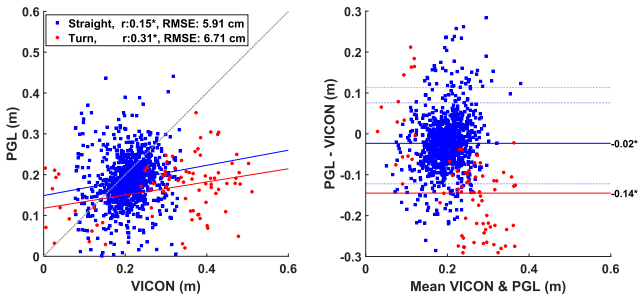

Fig. 7. Comparing step widths using correlation and Bland-Altman plots. Red circles are turning steps. *$p < 0.05$.

feet (ED) at the end of each step. Across all walking tasks, this was found to be 8.8 ± 1.0 cm on average.

The estimates of *SL*, *SW*, and *CW* for all tasks except AW are compared against the reference using Fig. 6, 7, and 8 respectively. Some steps had particularly large *SL* or *CW* values measured by the VICON© than the average, thereby skewing the distribution as outliers. They were removed based on the interquartile range of the distribution of the VICON© estimates for each parameter (*SL*, *SW*, and *CW*). Fig. 6, 7, and 8 distinguish between a step with relatively straight heading, denoted as a blue filled square and turning steps denoted by a red filled circle. In each of the three figures 6, 7, and 8, the left subplot shows the agreement between the PGL estimates and reference using correlations. The dotted gray line is the identity line, the solid blue line is the linear fit for the straight steps, and solid red line is the linear fit for the turning steps. The legends in each figure indicate the correlation between the PGL and reference and its significance denoted by a star. The average root mean square of the errors is also shown.

Further, in Fig. 6, 7, and 8, the right subplot shows the Bland-Altman plot. The solid lines denote the median difference between the two systems, with a star to denote no significant difference between the mean of the two systems. The dotted lines denote the 95% limits of agreement (LoA). The LoA for *SL* were found to be [−25.5 15.9] cm and [−24.7 37] cm for the straight and turning steps respectively. For *SW*, an LoA of [−16 11.6] cm and [−40.3 11.3], and for *CW* a value of [−9.5 1.6] and [−17.2 6.1] cm was found.

Finally, the feasibility of PGL in differentiating symmetric from asymmetric gait is shown in Fig. 9 and 10. These figures compare the boxplot distribution of *SL* on the left and right side. Fig. 9 plots this comparison for the NW task, where the subjects walked symmetrically, and Fig. 10 plots this for the asymmetric AW task. In both figures, the left subplot shows the distributions measured by the reference system, and the right subplot shows that of the PGL. Fig. 10 shows that the

TABLE IV
AVERAGE ROOT MEAN SQUARE OF THE ERRORS IN HORIZONTAL POSITIONS OF THE FEET AND COM, AND THE DIFFERENCES (*ED*) IN RELATIVE FOOT DISTANCES AT THE END OF EACH STEP

——	$Right_X(cm)$	$Right_Y(cm)$	$Left_X(cm)$	$Left_Y(cm)$	$CoM_X(cm)$	$CoM_Y(cm)$	$ED(cm)$
NW	12.7 ± 3.3	4.1 ± 1.3	11.2 ± 1.5	3.6 ± 0.7	8.3 ± 2.2	5.3 ± 1.4	9.3 ± 3.4
LW	12.7 ± 5.2	4.8 ± 0.6	11.6 ± 3.2	4.6 ± 1.1	8.8 ± 3.1	5.7 ± 0.8	9.4 ± 4.5
WT	12 ± 3.3	5.3 ± 2.1	11.3 ± 2.3	4.7 ± 1.3	7.8 ± 2.3	6.3 ± 1	8.9 ± 2.5
WT2	12.1 ± 3.6	5.4 ± 0.9	11.4 ± 1.6	4.6 ± 0.9	8.1 ± 1.9	7.1 ± 0.9	9.3 ± 2.3
SW	11.7 ± 3.9	5.7 ± 0.7	11.5 ± 2.3	5 ± 0.9	7.6 ± 2.4	7.5 ± 1.2	9.2 ± 1.1
AW	9.2 ± 3	4.9 ± 1.4	9.3 ± 1.6	4.1 ± 0.9	6.8 ± 1.9	5.5 ± 1.3	5.5 ± 2

NW: Normal Walk, LW: L Walk, WT: Walk and Turn, WT2: Walk and Turn Twice, SW: Slalom Walk, AW: Asymmetrical Walk.

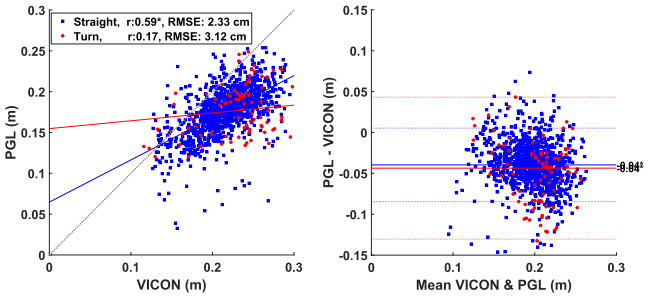

Fig. 8. Comparing CoM widths using correlation and Bland-Altman plots. Red circles are turning steps. $^*p < 0.05$.

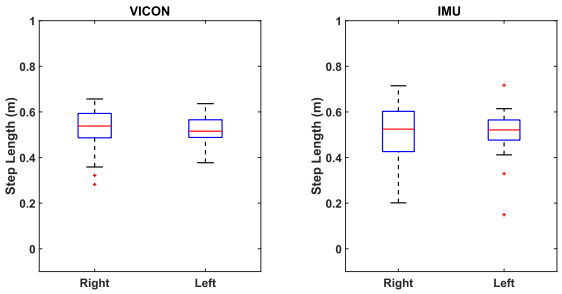

Fig. 9. Comparing distributions of right and left step lengths for the NW task.

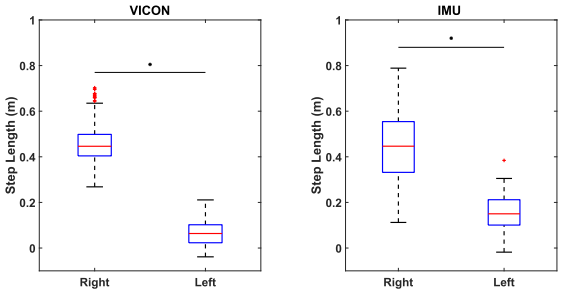

Fig. 10. Comparing distributions of right and left step lengths for the AW task. $^*p < 0.05$.

both, the reference and PGL, find significant differences in *SL* between the right and left side for the AW task.

IV. DISCUSSION

This study shows the feasibility of relying on simply a three IMU setup for estimating relative distances of the feet and CoM. Estimating kinetics [13], and kinematics using the principles in this study allows us to use the three IMU setup as a portable gait lab.

There are several biomechanical assumptions considered for this study. In order to apply (14), 3D GRF and height of CoM have to be estimated instantaneously. Refai *et al.* [13] have already discussed the feasibility of using the PGL in estimating 3D GRF while assuming that the CoM resides within the centroid of the pelvis. Here, the errors associated with the ratios ($rRat_{XZ}$, and $rRat_{YZ}$) as seen in Table III was $19.3 \pm 3.1\%$ of the range of the reference values in the worst case. The average RMS error in estimating the vertical CoM position by Floor-Westerdijk *et al.* [15] was 3.5 ± 1.3 mm. In our study, it was on average 7 ± 2.4 mm across all walking tasks. Though this is larger than the [15], they only compared the differences in a detrended position for an average stride. We state the average error in estimating the instantaneous CoM height over the complete gait including initiation, turning, and stopping. Knowledge of the force ratios and CoM height allows us to use the CMP constraint using (14) and (17). As the CMP measurement updates were applied only during specific instances of gait, the errors in estimating ratio of forces and CoM height influences the relative positions during these instances.

Fig. 5 shows the step-wise comparison of the tracking by the PGL for a subject performing the WT task. Each step is shown in its respective current step frame ψ_{cs}, with the feet and CoM moving from left to right. In some steps, for instance step 3, the trajectory of the stance (right) foot position measured by PGL is slightly different from the VICON©. This could be the rolling of the foot during stance phase, which is measured by VICON©. As the PGL tracks the foot as a fixed point, this rolling is not modelled during stance phase. Thus, we observe a steady medio-lateral position of the stance foot for the PGL estimates. Furthermore, although the virtual CMP point follows the trajectory of the Center of Pressure (CoP) [10], in (14) we assumed that it follows the trajectory of the stance foot tracked by the PGL. These two issues could induce a systematic difference in estimations of foot positions or spatial parameters of gait. The PGL could be further improved with a model for CoP movement [24] or the rolling of the stance foot. Further, we see more discrepancies during the turning steps than other steps. These issues could be because the movement of the CoM deviates further from the centroid of the pelvis when making turns.

Additional biomechanical constraints should be explored to improve estimation of kinematics during turning. Measuring the influence of the rotational inertia of the upper body could improve the assumptions of CMP. Nevertheless, the estimated positions converge to the reference values when the subject continues to make additional steps.

Table IV shows that the algorithm has comparable performances across different walking tasks in estimating the absolute position of the feet and CoM. As these errors are an average across all steps in a trial, they indicate the usefulness of PGL in restricting drift between the segments with time. Although marginal, the differences in the orientation of ψ_{cs} defined separately by the PGL and VICON© could influence these errors. The error margins can be put into perspective when comparing it against the average stride length, which was found to be 1.1 ± 0.2 m by VICON© for all tasks except AW. The mean absolute error in estimating stride lengths across all walking tasks was found to be 5.9 ± 1.5 cm in our study as compared to -1.5 ± 4.6 cm as found by Kitagawa and Ogihara [25]. Note that the errors in estimating positions for the AW task are similar to the others, even though this task comprised of an asymmetrical gait with shorter steps on the right. In our validation study [12] on the assumptions of CMP theory, we found that there was an average error of 6.7 ± 0.6 cm between the virtual CMP position and true foot position as measured by VICON©. These influence the errors in the relative distances (ED) between either feet as seen in Table IV. Sy *et al.* [9] used a set of biomechanical constraints to track the lower limb using a similar three IMU approach with an average error of 5.2 ± 1.4 cm. This was 13.5 ± 0.7 cm for our study. However, in the reference study [9], they assume a fixed pelvis, and measure all segments with respect to it. On the other hand, we track the relative distances between the feet and CoM for variable as well as asymmetric gait. The error margins include all steps in the walking task, thereby showing robustness against drift in relative distances, which becomes larger with time. It may be of interest to include the constraints explored in Sy *et al.* [9] where they also estimate joint kinematics. Combining Sy *et al.* [9] with the current study can result in a system that provides complete linear and joint kinematics of the lower limb using a minimal IMU setup.

We have also validated the PGL for estimating spatial parameters: *SL*, *SW*, and *CW* for variable gait. These parameters are dependent on good estimations of relative distances of both feet and CoM. In healthy subjects and hemiparetic populations, the *SL* variability is close to 2 cm and 3.4 cm respectively, and the *SW* variability is close to 2 cm and 1.8 cm respectively [26]. Using an ultrasound sensor to measure relative distances, Weenk *et al.* [3] estimated the *SL* and *SW* with an average absolute error of 1.7 ± 2 cm and 1.5 ± 1.5 cm respectively. In our study, using only three IMUs, we found it to be 4.6 ± 1.5 cm and 3.8 ± 1.5 cm respectively. These errors include variable walking, and are slightly larger than clinical variability. Analysing straight line walking tasks such as the 10 metre walk will reduce the impact of variable walking when using the PGL for clinical studies. Furthermore, although the estimates were significantly correlated with the reference system (Fig. 6, 7, and 8), the correlations were found to be moderate for estimations of *SL*, and *CW*, and weak for the *SW*. This suggests that there is merit in using the PGL to study average spatial parameters over a number of trials, although caution must be taken when comparing individual steps.

Figures 6, 7, and 8 do not include the spatio-temporal parameters for AW task, as the steps were asymmetric on either side. The spread of the spatio-temporal parameters for straight steps in the correlation subplot in all three figures lies along the identity line. The bias seen in the Bland-Altman plots could be due to systematic differences owing to the several assumptions considered and discussed in this study.

Finally, Fig. 9 and 10 show that the algorithm can distinguish between normal and asymmetric walking patterns, as identified by significant differences in step lengths for the AW task. This indicates that the PGL may be adequately sensitive for differences of clinical importance such as gait asymmetry due to stroke or other conditions.

A. Limitations and Future Work

The PGL requires reliable estimations of the CoM height and velocity, feet velocities, and 3D GRF before it can track the relative distances. Therefore, a number of assumptions were used regarding the biomechanics of gait. For instance, in (13), we found the average height of CoM during walking by optimizing the errors between the PGL estimate and reference values. Further, we used an inverted pendulum model of walking where the CoM is encompassed within the pelvis segment [15]. There may be larger errors if the CoM deviates further from the centroid of the pelvis, or if the subject crouches or jumps. Errors may also be larger for subjects with an asymmetric body posture due to an impairment or paralysis.

Applying the PGL requires knowledge of initial relative distances of the feet and CoM, which could be input using a tape or other sources. Further, the algorithms require a few steps to calibrate and define the different reference frames, and to initialise the heading of the feet. This could mean that there are some restrictions to be considered when designing a real time application system. The current design of the sensor fusion filter tracks 18 parameters for each iteration that includes the position and velocity of each foot and CoM, and might result in a heavy computational load. However, this should not pose a problem if the processing is performed offline, on a desktop, or a cloud service. Further, it is important that the three IMUs are synchronized well, as the movements are related to each other.

The PGL has not been tested on other aspects of variable gait such as shuffling of the feet, ascending or descending stairs, walking backwards, etc. Although, we have shown that the errors are close to margins of variability, they can be improved, and a follow up study with measurements from a free daily life environment must be designed. The error margins found in the current PGL could be acceptable to derive an overview of gait patterns, track people in daily life, and also to derive balance and stability measures using the relative foot distances. For instance, the BoS and MoS [1] can be derived using this approach. However, employing the PGL to study

individual steps must be considered within the provided error margins.

Here, the AW task was used to validate the feasibility of using PGL in asymmetric gait. Nevertheless, a validation study using subjects with impaired and/or asymmetric gait is required, as it might be difficult to detect distinct gait events in impaired gait. Issues with lower limb motor control may result in shuffling patterns, such as freezing of gait as seen in patients with Parkinson's disease. This will influence the estimation of gait events, and therefore the application of CMP updates.

V. Conclusion

The feasibility of using a minimal three IMU based setup in measuring relative distances between the feet and CoM is shown for overground variable gait. The average absolute errors in estimating step lengths and step widths were 4.6 ± 1.5 cm and 3.8 ± 1.5 cm respectively. The approach is sensitive in differentiating symmetric and asymmetric gait. Further validation in free walking conditions and subjects with impaired gait patterns must be done.

Acknowledgment

The authors thank Ed Droog, Marcel Weusthof (University of Twente), and Leendert Schaake (Roessingh Research and Development) for assisting with the measurement setups.

References

[1] F. B. van Meulen, D. Weenk, J. H. Buurke, B.-J. F. van Beijnum, and P. H. Veltink, "Ambulatory assessment of walking balance after stroke using instrumented shoes," *J. Neuroeng. Rehabil.*, vol. 13, no. 1, p. 48, Dec. 2016.

[2] D. Roetenberg, H. Luinge, and P. Slycke, "Xsens MVN: Full 6DOF human motion tracking using miniature inertial sensors," Xsens Technol., Enschede, The Netherlands, Tech. Rep., 2009.

[3] D. Weenk, D. Roetenberg, B.-J. F. van Beijnum, H. J. Hermens, and P. H. Veltink, "Ambulatory estimation of relative foot positions by fusing ultrasound and inertial sensor data," *IEEE Trans. Neural Syst. Rehabil. Eng.*, vol. 23, no. 5, pp. 817–826, Sep. 2015.

[4] S. Bertuletti, U. Della Croce, and A. Cereatti, "A wearable solution for accurate step detection based on the direct measurement of the inter-foot distance," *J. Biomech.*, vol. 84, pp. 274–277, Feb. 2019.

[5] I. Skog, J.-O. Nilsson, D. Zachariah, and P. Handel, "Fusing the information from two navigation systems using an upper bound on their maximum spatial separation," in *Proc. Int. Conf. Indoor Positioning Indoor Navigat. (IPIN)*, Nov. 2012, pp. 13–15.

[6] X. Niu, Y. Li, J. Kuang, and P. Zhang, "Data fusion of dual foot-mounted IMU for pedestrian navigation," *IEEE Sensors J.*, vol. 19, no. 12, pp. 4577–4584, Jun. 2019.

[7] J. Bancroft and G. Lachapelle, "Twin IMU-HSGPS integration for pedestrian navigation," in *Proc. 21st Int. Tech. Meeting Satell. Division Inst. Navigat. (ION GNSS)*, 2008, pp. 16–20.

[8] H. Zhao *et al.*, "Heading drift reduction for foot-mounted inertial navigation system via multi-sensor fusion and dual-gait analysis," *IEEE Sensors J.*, vol. 19, no. 19, pp. 8514–8521, Oct. 2019.

[9] L. Sy *et al.*, "Estimating lower limb kinematics using a reduced wearable sensor count," 2019, *arXiv:1910.00910*. [Online]. Available: http://arxiv.org/abs/1910.00910

[10] M. B. Popovic, A. Goswami, and H. Herr, "Ground reference points in legged locomotion: Definitions, biological trajectories and control implications," *Int. J. Robot. Res.*, vol. 24, no. 12, pp. 1013–1032, Dec. 2005.

[11] H. M. Schepers, E. H. F. van Asseldonk, J. H. Buurke, and P. H. Veltink, "Ambulatory estimation of center of mass displacement during walking," *IEEE Trans. Biomed. Eng.*, vol. 56, no. 4, pp. 1189–1195, Apr. 2009.

[12] M. I. Mohamed Refai *et al.*, "Portable gait lab: Zero moment point for minimal sensing of Gait*," in *Proc. 41st Annu. Int. Conf. IEEE Eng. Med. Biol. Soc. (EMBC)*, Jul. 2019, pp. 2077–2081.

[13] M. I. Mohamed Refai, B.-J. F. van Beijnum, J. H. Buurke, and P. H. Veltink, "Portable gait lab: Estimating 3D GRF using a pelvis IMU in a foot IMU defined frame," *IEEE Trans. Neural Syst. Rehabil. Eng.*, vol. 28, no. 6, pp. 1308–1316, Jun. 2020.

[14] M. Zok, C. Mazza, and U. Della Croce, "Total body centre of mass displacement estimated using ground reactions during transitory motor tasks: Application to step ascent," *Med. Eng. Phys.*, vol. 26, no. 9, pp. 791–798, Nov. 2004.

[15] M. J. Floor-Westerdijk, H. M. Schepers, P. H. Veltink, E. H. F. van Asseldonk, and J. H. Buurke, "Use of inertial sensors for ambulatory assessment of Center-of-Mass displacements during walking," *IEEE Trans. Biomed. Eng.*, vol. 59, no. 7, pp. 2080–2084, Jul. 2012.

[16] M. I. Mohamed Refai, B.-J. F. van Beijnum, J. H. Buurke, and P. H. Veltink, "Portable Gait Lab: Instantaneous centre of mass velocity using three inertial measurement units," in *Proc. IEEE SENSORS*, Oct. 2020.

[17] I. Skog, P. Händel, J.-O. Nilsson, and J. Rantakokko, "Zero-velocity detection—An algorithm evaluation," *IEEE Trans. Biomed. Eng.*, vol. 57, no. 11, pp. 2657–2666, Nov. 2010.

[18] G. Pacini Panebianco, M. C. Bisi, R. Stagni, and S. Fantozzi, "Analysis of the performance of 17 algorithms from a systematic review: Influence of sensor position, analysed variable and computational approach in gait timing estimation from IMU measurements," *Gait Posture*, vol. 66, pp. 76–82, Oct. 2018.

[19] G. Welch and G. Bishop, "An introduction to the Kalman filter," Dept. Comput. Sci., Univ. North Carolina Chapel Hill, Chapel Hill, NC, USA, Tech. Rep. TR 95-041, 1995.

[20] P. H. Veltink, C. Liedtke, E. Droog, and H. van der Kooij, "Ambulatory measurement of ground reaction forces," *IEEE Trans. Neural Syst. Rehabil. Eng.*, vol. 13, no. 3, pp. 423–427, Sep. 2005.

[21] A. L. Hof, "Scaling gait data to body size," *Gait Posture*, vol. 4, no. 3, pp. 222–223, May 1996.

[22] M. Benoussaad, B. Sijobert, K. Mombaur, and C. Azevedo Coste, "Robust foot clearance estimation based on the integration of foot-mounted IMU acceleration data," *Sensors*, vol. 16, no. 1, p. 12, Dec. 2015.

[23] F. Huxham, J. Gong, R. Baker, M. Morris, and R. Iansek, "Defining spatial parameters for non-linear walking," *Gait Posture*, vol. 23, no. 2, pp. 159–163, Feb. 2006.

[24] M. I. Mohamed Refai, B.-J. F. van Beijnum, J. H. Buurke, and P. H. Veltink, "Gait and dynamic balance sensing using wearable foot sensors," *IEEE Trans. Neural Syst. Rehabil. Eng.*, vol. 27, no. 2, pp. 218–227, Feb. 2019.

[25] N. Kitagawa and N. Ogihara, "Estimation of foot trajectory during human walking by a wearable inertial measurement unit mounted to the foot," *Gait Posture*, vol. 45, pp. 110–114, Mar. 2016.

[26] C. K. Balasubramanian, R. R. Neptune, and S. A. Kautz, "Variability in spatiotemporal step characteristics and its relationship to walking performance post-stroke," *Gait Posture*, vol. 29, no. 3, pp. 408–414, Apr. 2009.